Clays and Clay Minerals, Vol. 66, No. 5, 426–437, 2018.

EXPERIMENTAL AND ATOMIC MODELING OF THE ADSORPTION OF ACID AZO DYE 57 TO SEPIOLITE

DENİZ KARATAŞ[1], DILEK SENOL-ARSLAN[2], AND ORHAN OZDEMIR[2,*]

[1]Istanbul Technical University, Mineral Processing Engineering Department, 34469, Maslak, Istanbul, Turkey
[2]Istanbul University, Mining Engineering Department, 34320, Avcilar, Istanbul, Turkey

Abstract—Sepiolite is a hydrated magnesium silicate with a microporous and mesoporous structure. The fibrous morphology and the alternating blocks and tunnels along the fiber direction of sepiolite make it an ideal material to sequester a variety of organic and inorganic contaminants. The adsorption of various surfactants by organo sepiolites have been experimentally investigated. How this hydrophobic material adsorbs dye molecules at the atomic level, however, is a great mystery. For this reason, the present study focused on the adsorption of acid azo 57 dye molecules to modified sepiolite. For this purpose, the amenability of sepiolite to remove the anionic textile dye (acid azo red dye 57) was first studied in detail. Additionally, a typical cationic surfactant, hexadecyltrimethylammonium Br (HTAB), was used to modify sepiolite to increase the adsorption capacity. Zeta potential measurements on the sepiolite and the HTAB modified sepiolite were also carried out. Moreover, Density Functional Theory (DFT) studies were performed to understand the mechanism of the adsorption of dye molecules to natural and modified sepiolite surfaces. On the basis of the experimental studies, three general systems were theoretically examined: (i) HTAB molecules on sepiolite basal surfaces to represent four Si tetrahedra, (ii) neutral or charged acid azo red dye 57 molecules on sepiolite basal surfaces to represent four Si tetrahedra, and (iii) HTAB on the surface of neutral or charged acid azo red dye 57 molecules as a substrate. The results clearly indicated good agreement between the experimental studies and the theoretical computational DFT studies. For example, the double layer structure found in experimental studies was also demonstrated in DFT studies and confirmed increased adsorption in the presence of acid azo dye 57.

Key Words—Adsorption, B97-D/TZVP, Density Functional Theory (DFT), Hexadecyltrimethylammonium Bromide (HTAB), Sepiolite, Textile Dyes.

INTRODUCTION

Textile industries discharge wastewater that originates from dyeing and finishing processes. Major pollutants include aqueous suspensions that are highly colored, have large amounts of suspended solids, and contain dissolved organic chemicals (Chern and Huang, 1998; Al-Degs *et al.*, 2000; Yoo *et al.*, 2001; Duman *et al.*, 2015). Color removal from textile effluents, therefore, has received great attention in the last few decades due to the toxicity and visibility of these pollutants (ICI Watercare, 1991).

Reactive dyes are generally used in dyeing processes, but ~20 to 40% of the dyes remain in the effluents (Rearick *et al.*, 1997; Wu *et al.*, 1998). The dyes are highly soluble in water and for this reason removal from wastewater is difficult by conventional coagulation and activated sludge processes (Chern and Huang, 1998). The two major technologies available for wastewater treatment in the textile industry are oxidation and adsorption. Oxidation methods, such as ultraviolet (UV) light, ozone, and UV/H_2O_2 treatments, are some of the methods used to totally eliminate organic C in wastewater (Huang and Shu, 1995). Adsorption is rapidly becoming a prominent method to treat aqueous effluents and has been extensively used in industrial processes for a variety of separation and purification purposes, especially for the removal of colored and colorless organic pollutants from industrial wastewater (Al-Qodah, 2000). Activated C and polymer resins appear to be the best adsorbents to remove waste chemicals from relatively concentrated wastewater, but these materials are expensive and must be regenerated to limit the expense (McKay *et al.*, 1982; Meshko *et al.*, 2001; Hu *et al.*, 2013). In a search for less expensive materials, several studies have focused on more cost-effective adsorbent systems, which include natural clays for use with reactive and acid dyes (El-Geundi, 1991), chitosan for vinyl sulfone and chlorotriazine reactive dyes (Juang *et al.*, 1997; Oladipo *et al.*, 2015), sunflower stalks for basic dyes (Sun and Xu, 1997), sepiolite for rhodamine (Arbeloa *et al.*, 1997), shale oil ash for azo dyes (Al-Qodah, 2000), montmorillonite and sepiolite for methyl green (Rytwo *et al.*, 2000), and natural and modified zeolites for basic dyes (Meshko *et al.*, 2001; Benkli *et al.*, 2005).

Sepiolite is a natural fibrous clay mineral with a hydrated Mg silicate structure and a high surface area (Alvarez, 1984; Aznar *et al.*, 1992; Galan, 1996, Ruiz-Hitzky, 2001; Suarez and Garcia-Romero, 2012; Gür *et*

* E-mail address of corresponding author:
orhanozdemir@istanbul.edu.tr
DOI: 10.1346/CCMN.2018.064109

al., 2015). The fibers of sepiolite are constructed from tetrahedral and octahedral units (Santaren, 1993; Ruiz-Hitzky, 2001) and are represented by the half unit-cell formula $Si_{12}O_{30}Mg_8(OH,F)_4{\cdot}8H_2O$ (Brauner and Preisinger, 1956; Santaren *et al.*, 1990). Sepiolite has special features, such as a high surface area, a fiber structure, high porosity, tunnels and channels, a unique crystal morphology, and high surface activity. It forms stable high-viscosity suspensions at low solids concentration (Sabah, 1998; Lemic *et al.*, 2005). The physical and chemical properties of sepiolite can be improved by heat or acid treatments (Alvarez, 1984; Galan, 1996; Sabah, 1998; Cinar *et al.*, 2011). It is, therefore, useful in many technologies, and plays a role in sorptive, catalytic, and rheological processes (Alvarez, 1984; Murray, 1991, 2000; Galan, 1996). In addition, the unique sepiolite structure is sensitive to applied mechanical stresses, which can result in structural and dimensional changes (Cornejo and Hermosin, 1988; Can *et al.*, 2010).

In recent years, many theoretical studies on clay mineral-surfactant relationships have been published that include kaolinite, montmorillonite, and sepiolite (Pelmenschikov and Leszczynski, 1999; Karatas *et al.*, 2013, 2017; Kasprzhitskii *et al.*, 2016). No atomic-level theoretical or experimental study, however, has focused on the adsorption of azo dyes to sepiolite. The aim of the present study was, therefore, to investigate the adsorption mechanism of acid azo dye 57 to natural and modified (HTAB) sepiolite surfaces using both experimental (electrokinetics and adsorption) and theoretical (Density Functional Theory, DFT) methods.

MATERIALS AND METHODS

Materials

The natural sepiolite sample used as an adsorbent in the present study was obtained from the Sivrihisar region of Eskisehir, Turkey. The sample was first ground to less than 63 μm for the adsorption experiments. The particle size distribution ($d_{50} \cong 7$ μm) was measured using a Malvern Mastersizer 2000 (Malvern Instruments Ltd, Worcestershire, UK). A chemical analysis of the sepiolite is presented in Table 1. Mineralogical analysis using a Rigaku D-max 2200 X-ray powder diffractometer (Rigaku, Tokyo, Japan) indicated that the sample mostly contains sepiolite along with minor impurities, such as calcite and dolomite. The reactive dye (acid azo dye 57, $C_{24}H_{21}N_4NaO_6S_2$) was used for the adsorption experiments and was obtained from Reinleder OK Chemistry, Istanbul, Turkey. The quaternary amine, hexadecyltrimethylammonium bromide (HTAB, $C_{19}H_{42}BrN$), was used to modify the surface of the sepiolite. The HTAB was purchased from Sigma Aldrich (St. Louis, Missouri, USA) and was specified to be of 99% purity with a molecular weight of 346.46 g/mol. The modification procedure briefly involved the mixing of 5% sepiolite solids with a 2×10^{-2} mol/L solution of HTAB followed by equilibration, solid-liquid separation, and drying as described by Armagan *et al*. (2003a). The pH was adjusted using analytical grade HCl and NaOH (Merck KGaA, Darmstadt, Germany). Deionized (DI) water (18 MΩ-cm) was freshly purified using a setup consisting of a reverse osmosis unit and an Ultrapure Academic Milli-Q system (Millipore Ltd, Molshem, France) and was used for all studies. The surface tension of the DI water was measured and found to be about 72.0 mN/m at 23°C.

Methods

Electrokinetic studies. The electrokinetic properties of the sepiolite sample with and without the dye molecules were determined using a ZetaPlus zeta potential analyzer (Brookhaven Instrument Corporation, Holtsville, New York, USA). The ZetaPlus unit automatically calculates the electrophoretic mobility of particles and then converts the electrophoretic mobility values into the zeta potential using the Smoluchowski equation:

$$\zeta = \frac{\eta\mu}{\varepsilon} \quad (1)$$

where ζ is the zeta potential, η is the dynamic viscosity of the fluid, μ is the particle mobility, and ε is the dielectric constant.

Natural and modified sepiolite samples (0.1 g) were conditioned in 100 mL of distilled water for 15 min (0.1% solids). The suspension pH was adjusted by the addition of 0.1 mol/L HCl or NaOH and the suspensions were left undisturbed for 10 min to let the larger particles settle. Finally, twenty zeta potential measurements over a pH range from 3 to 11 were performed and the average zeta potential value at each pH was obtained for the sepiolite particles with all measurements made at ambient temperature (22±1°C).

Adsorption studies. The adsorption experiments were conducted in 10-mL glass vials using a 0.1% solids content for the modified sepiolite suspensions and dye

Table 1. Chemical composition of sepiolite.

Compound	SiO_2	Al_2O_3	Fe_2O_3	MgO	CaO	Na_2O	K_2O	TiO_2	P_2O_5	MnO	Cr_2O_3	LOI*
Wt.%	44.42	2.36	0.95	19.87	2	–	0.33	0.13	0.01	0.01	–	29.76

*LOI: Loss on ignition.

https://doi.org/10.1346/CCMN.2018.064109 Published online by Cambridge University Press

concentrations that ranged from 10 to 1000 mg/L. The bottles were placed on an IKA orbital shaker (IKA, Wilmington, North Carolina, USA) agitated at 400 rpm at room temperature for 4 h followed by centrifugation at 2800 × g for 5 min to separate the solids from the supernatants. The equilibrium concentrations of the dye in the supernatants were determined using a T80 UV/VIS spectrophotometer (PG Instruments Limited, Leicestershire, UK) at 542 nm. The adsorption capacity (q_e) was calculated as follows:

$$q_e = \frac{(C_i - C_e) * V}{m} \quad (2)$$

where q_e is the amount of dye adsorbed per gram of adsorbent in mg/g; C_i is the initial dye concentration in mg/L; C_e is the equilibrium (residual) dye concentration in mg/L; V is the volume of the solution in L; and m is the mass of adsorbent (g).

Density Functional Theory (DFT) Studies

Models setup. The adsorption mechanism of the dye to the natural and modified sepiolite samples was investigated using Density Functional Theory (DFT). In the case of DFT, total and interaction (adsorption) energies of the systems were computed using the PBE/TZVP and B97-D/TZVP basis sets, respectively. Given that the induced dipole interaction is due to fluctuations in the electron distribution during interactions between the molecules, the dispersion contribution was considered (Stefan, 2006). Therefore, a popular, new, and faster functional B97-D *via* the TZVP basis set was chosen to calculate interaction energies. All theoretical studies were performed in vacuum and solvent media using the *TURBOMOLE V6.1* software (Ahlrichs *et al.*, 1989) package. At first, all models were optimized under vacuum using the Perdew, Burke, and Ernzerhof (PBE) (Perdew *et al.*, 1996) functional with the TZVP basis set. Water was then added implicitly as a solvent *via* the *COSMO* program module and all models were again optimized using the same basis sets. After each geometric optimization step, the interaction energy of each model was computed.

Karatas *et al*. (2013) investigated quaternary amine adsorption to sepiolite surfaces both theoretically and experimentally. In the Karatas *et al*. (2013) study, the Mg was discussed in detail and the results indicated that the constructed model was distorted during the studies. Additionally, Karatas *et al*. (2013) stated that the Mg layer did not significantly affect the basal surface interactions. Moreover, in order to reduce the quantum computation time, the Mg layer was neglected and model studies with the structure in Figure 1 were carried out. The structures used in theoretical investigations searched for both HTAB alkyl chain-chain and HTAB head-surface interactions and the system was generated as a combination of the structures. The number of HTAB surfactant molecules was determined for two reasons. One reason was to explain and compare the interactions of the HTAB hydrophobic tails. The second reason depends on the mineral surface area required per HTAB molecule, which was roughly calculated to find the number of adsorbed HTAB surfactant molecules. For example, the maximum width and length of the HTAB surfactant head group is 3.69×4.26 Å^2. Similarly, the surface areas of the acid azo dye 57 molecules and silica tetrahedra are 128.81 and 247.66 Å^2, respectively. The

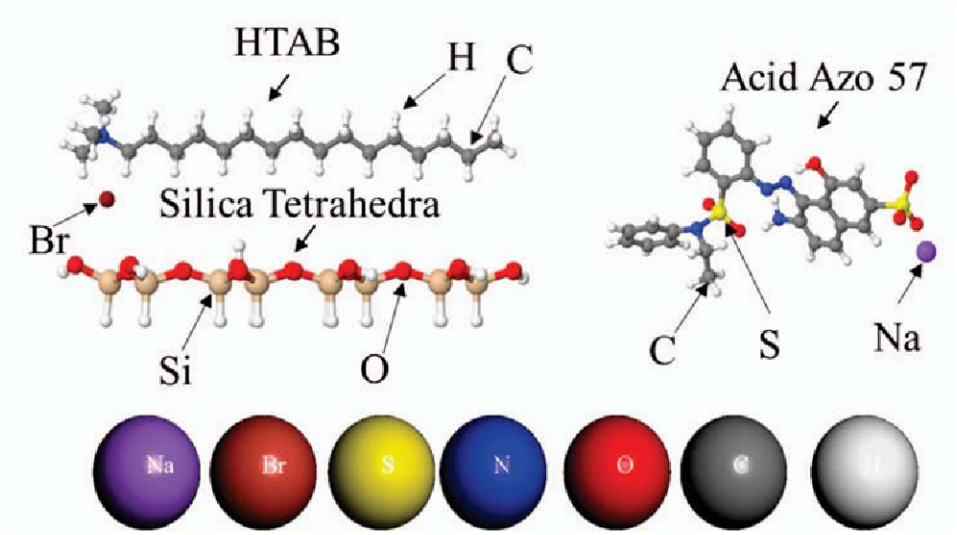

Figure 1. Representative ball and stick models for HTAB, silica tetrahedra, and acid azo dye 57. The white (H, white), melon yellow (Si, light gray), red (O, black), blue (N, black), baroque red (Br, black), gray (C, black), yellow (S, gray), and purple (Na, black) colors represent the elements indicated in parentheses with the grayscale appearance.

https://doi.org/10.1346/CCMN.2018.064109 Published online by Cambridge University Press

surfactant head group surface area was divided by the surface areas of the acid azo dye 57 and the silica tetrahedra to roughly calculate the number of surfactant molecules. This was calculated to be 2.6 and 4.9 molecules for each surface, but only 3 surfactant molecules were placed on the surfaces in the models.

In this perspective, the representative parts of the structures were experimentally considered to be in a water environment. Therefore, five models were built to explain interactions of acid azo dye 57 and HTAB molecules with sepiolite and compare to the experimental results. Experimental results revealed that the lowest probability of interaction was observed between acid azo dye 57 and sepiolite so the interactions between dye and sepiolite were modeled first. In the second model, 3 HTAB molecules with and without Br^- ions were placed onto 4 silica tetrahedra generated from the sepiolite unit cell (Post *et al.*, 2007). In the third and fourth models, interactions between modified silica tetrahedra with 2 HTAB molecules and acid azo dye 57 were computed. In the final model, interactions between three HTAB molecules and an acid azo dye 57 molecule were run and modeled. To relax the surface, all dangling atoms were saturated with H for the structures shown in Figure 1.

Computational methods. In this section, to better understand adsorption, explain the electrostatic interactions, and explain hydrogen bonding between the structures, the interaction energies (equation 3) using the B97-D/TZVP basis set were calculated. Adsorption configurations contained many atoms; therefore, the resolution of the identity (RI) (Eichkorn, 1995) approximation for all geometric optimizations was used and all atomic positions were relaxed and followed by interaction energy calculations performed using the B97-D functional with the dispersion contribution from the TZVP basis set. To minimize the basis set superposition error, the counter-poise (CP) method (Boys and Bernardi, 2002) was used and the interaction energies calculated using the equations below:

$$E_{BE}^{CP} = E_{dye\ +\ Surf}^{(dye\ +\ Surf)} - (E_{dye}^{(dye\ +\ Surf)} + E_{Surf}^{(dye\ +\ Surf)}) \quad (3)$$

In equation 3, the counter-poise corrected (CP) binding energy formula was used to calculate the binding energy between the acid azo dye and HTAB, where within the same basis $E_{dye\ +\ Surf}^{(dye\ +\ Surf)}$, $E_{dye}^{(dye\ +\ Surf)}$, and $E_{Surf}^{(dye\ +\ Surf)}$ are the total energies of all the fragments, the acid azo dye 57 molecules, and the HTAB molecules in kJ/mol, respectively.

$$E_{BE}^{CP} = E_{tetrahedron\ +\ Surf}^{(tetrahedron\ +\ Surf)} - (E_{tetrahedron}^{(tetrahedron\ +\ Surf)} + E_{Surf}^{(tetrahedron\ +\ Surf)}) \quad (4)$$

In equation 4, the counter-poise corrected (CP) binding energy formula was used to calculate the binding energy between silica tetrahedra and HTAB molecules, where within the same basis, $E_{tetrahedron\ +\ Surf}^{(tetrahedron\ +\ Surf)}$, $E_{tetrahedron}^{(tetrahedron\ +\ Surf)}$, and $E_{Surf}^{(tetrahedron\ +\ Surf)}$ are, respectively, the total energies of all fragments, acid azo dye 57, and HTAB molecules in kJ/mol and the corresponding energies are presented in Table 3.

RESULTS AND DISCUSSION

Electrokinetic Properties of Sepiolite

Sepiolite undergoes acid-base interactions in the vicinity of pH 8.5 and, thus, exhibits a strong buffering capacity, particularly at acidic pHs. A minute was long enough for a sepiolite suspension adjusted to pH 3 to regain the natural pH of 8.5 with Mg released into solution (Ozdemir *et al.*, 2007). Characterization of the electrokinetic behavior of natural and modified sepiolite (Figure 2) revealed that the point of zero charge (pzc) for natural sepiolite was 3.2 at a 0.1% solids content and that the negative charge prevailed at the natural sepiolite suspension pH of 8.5. The modified sepiolite charge was positive at all pH values, which indicated that HTAB in excess of the cation exchange capacity was adsorbed to the sepiolite surfaces.

Moreover, reactive dyes, such as acid azo dye 57, contain negatively charged sulfonate azo groups in equilibrium with the free acid. The sulfonate groups are, thus, repelled by negatively charged mineral surfaces. The results for the modified sepiolite (0.1%) revealed that the surface acquired a positive charge and, consequently, became receptive to electrostatic attraction of the negatively charged dye molecules. Dissociated hydroxyl groups on the dye molecule may also weakly compete with the sulfonate groups for positive charge sites on the clay mineral, but competitive adsorption is expected to favor the sulfonate groups (Ozdemir *et al.*, 2004).

These results clearly indicated that the surfaces of natural sepiolite modified with HTAB not only made the surfaces of sepiolite hydrophobic, but also neutralized the negative charge (Shuali *et al.*, 1989; Sabah and Celik, 2002; Sabah *et al.*, 2002) as long as the dye

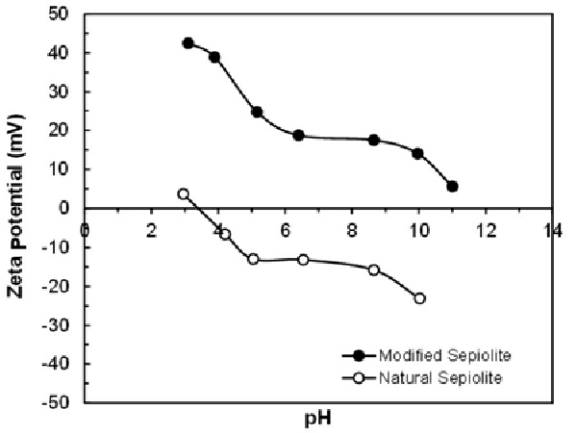

Figure 2. Plot of zeta potential *vs*. pH of natural and modified sepiolite samples at a 0.1% solids suspension concentration.

https://doi.org/10.1346/CCMN.2018.064109 Published online by Cambridge University Press

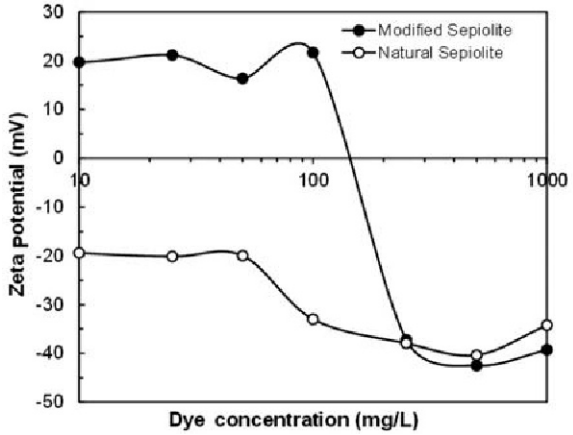

Figure 3. Zeta potentials of the natural and modified sepiolite samples as a function of dye concentration.

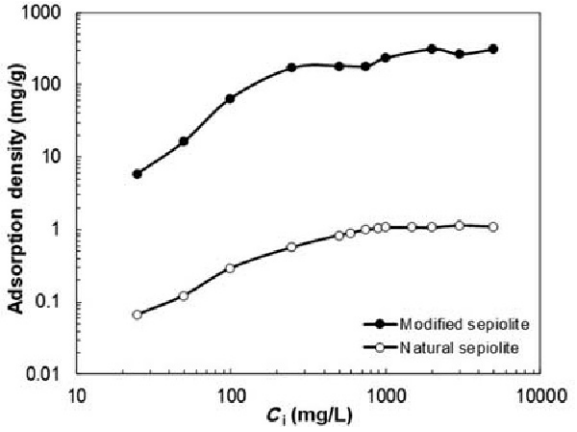

Figure 4. Adsorption isotherms of natural and modified sepiolite plus acid azo dye 57 systems at the natural sepiolite pH of 8.5.

concentration was greater than about 125 mg/L dye concentration, which was also the pzc. At dye concentrations >125 mg/L, the sepiolite surface rapidly acquired a negative charge and a maximum dye concentration of about 500 mg/L was reached. Additionally, the zeta potential of natural sepiolite was always negative (Figure 3) and became even more negative with increasing dye concentration, which partially explains why the number of dye molecules that accumulated on the natural sepiolite was less than on the HTAB-modified sepiolite. The greater hydrophobicity of the HTAB-modified sepiolite, as reported in a previous study (Ozdemir *et al.*, 2004), also enhanced dye adsorption to it.

Adsorption of acid azo dye 57

A series of acid azo dye 57 adsorption experiments were carried out at different solids concentrations of both the natural and HTAB-modified sepiolites. Sepiolite suspension concentrations of >0.1% solids will separate from suspension, so the adsorption experiments were conducted below that threshold to avoid sedimentation (Ozdemir *et al.*, 2004). The dye adsorption capacity of natural sepiolite (Figure 4) increased to 1.1 mg/g as dye concentrations increased up to 1000 mg/L, above which the adsorption capacity remained almost steady. The same trend was also obtained for the HTAB-modified sepiolite in that the dye adsorption capacity increased to 307.4 mg/g as dye concentrations were increased up to 2000 mg/L, then remained nearly constant. Modification of sepiolite with HTAB, therefore, substantially improved the adsorption of acid azo dye 57 by about 300 fold.

Interactions between azo acid 57 and sepiolite (silica tetrahedra). In this section, two theoretical approaches were used to model the adsorption of acid azo dye 57 to the silica tetrahedra of sepiolite. The silica tetrahedral configuration used was identical in all calculations. The same acid azo dye was also used, but the negatively charged O groups were saturated with H as shown by the oval dashed line in the upper model shown in Figure 5. The models shown in Figure 5 contain 129 and 128 atoms, respectively. The dyestuffs in the models were well adsorbed to the silica tetrahedra *via* H-bonds. In some cases, the H-bonds were formed by H and O atoms between surfaces as well as by H atoms attached to the O atoms of silica tetrahedra and to the O atoms of -SiOH. Related bond distances were calculated to be between 2.59 and 2.90 Å.

All the bonds distances in Figure 5 indicated that the dye molecules in the negatively charged model were closer to the silica tetrahedra. Greater curling by the N in the middle part of the acid azo dye 57 molecule in the lower part of Figure 5 also supports this conclusion. The 2.01 Å distance between N and H in the first model cannot occur in the second model. In brief, all observations indicate that acid azo dye 57 can hydrogen bond to the silica tetrahedra. Further, the sulfonate group is attracted more strongly than the N group, as indicated in previous work (Benkli *et al.*, 2005) on the adsorption of dye molecules (Reactive Black 5, Red 239, and Yellow 176) to a zeolite modified with HTAB.

Interactions between HTAB and sepiolite (silica tetrahedra). To explain HTAB interactions with or adsorption to silica tetrahedra, 2 models were built. One of the models was a neutral system, which was neutralized by three Br^- ions. The second model was built without Br^- ions. The Br^- ions were added to the system for a better comparison and to explain the effect of ions on the adsorption phenomenon. The neutralized and optimized system with an implicit water media is illustrated in Figure 6.

After the DFT computation (Figure 6, a modified sepiolite structure with 260 atoms and 3 Br^- ions), two important conclusions emerged. First, the interactions among the aliphatic CH_2 group tails, even if surrounded by water, might have been limited by steric hindrance.

https://doi.org/10.1346/CCMN.2018.064109 Published online by Cambridge University Press

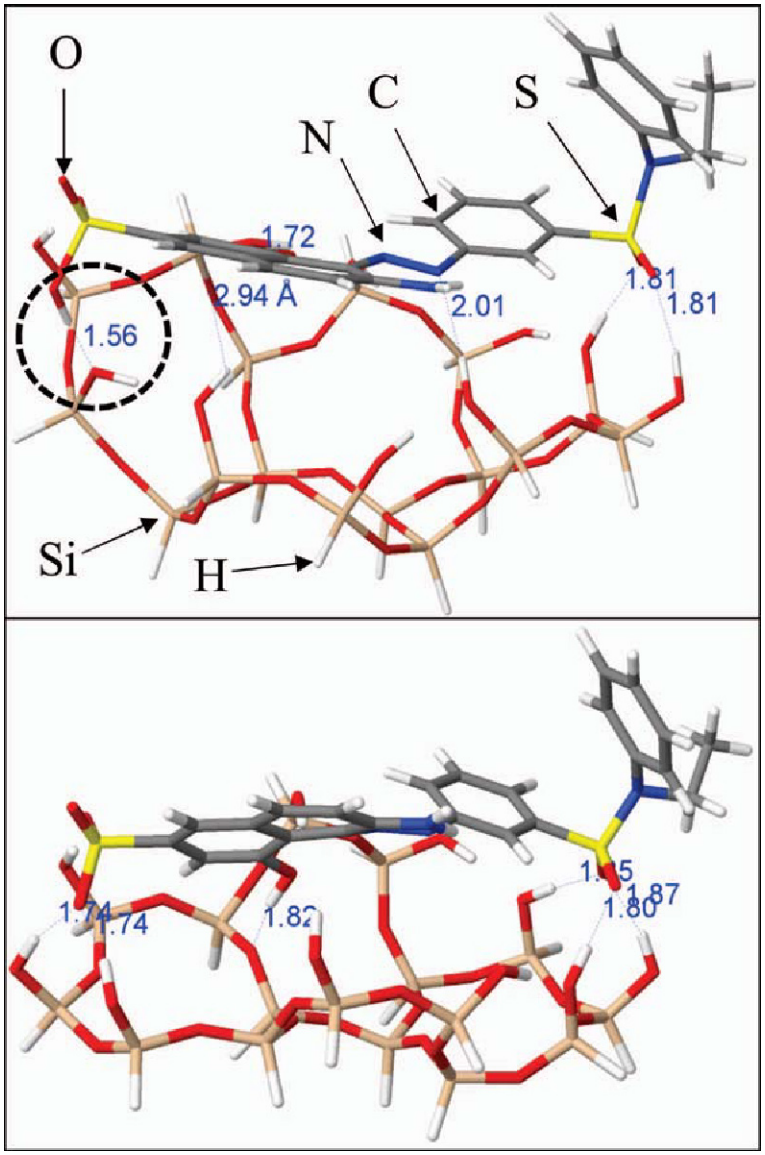

Figure 5. Final states of the optimized structures in an implicit water media between acid azo dye 57 and silica tetrahedra. The white (H, white), red (O, black), blue (N, black), gray (C, black), melon yellow (Si, light gray), and yellow (S, gray) colors represent the elements indicated in parentheses with the grayscale appearance.

The second conclusion was that because Br^- ions were added to the system, the surfactant head groups did not leave with each other. In this case, Br^- ions were electrostatically bound to the positively charged head groups. Both the hydrophobic interactions between $-CH_2$ aliphatic groups (*i.e.* HTAB hydrophobic tails) and the repulsive forces between polar head groups acted to optimize the model (Figure 6). In addition, Br^- ions act to stabilize HTA^+ adsorbed to sepiolite surfaces. On the other hand, HTAB can adsorb to the tetrahedral −SiOH groups. For this reason, Br^- ions and the H bonded to C atoms can bind to the H and O of −SiOH groups, respectively. All intermolecular and intramolecular interactions are presented in Table 2, which include all the H bonds between the enumerated surfactant Br^- ions, the H bonded to C atoms, and the H/O atoms of −SiOH groups. All intermolecular distances changed from 2.18 to 2.99 Å. Notice also from Table 2 that all H-bonds that belong to Br^- ions interacted between the sepiolite surface and HTAB surfactant head group. For example, 190 numbered Br^- ions interacted with 44 numbered H atoms of silica surface −SiOH groups due to the 2.22 Å distance. The intramolecular H-bonds between the H and O atoms of −SiOH were stronger as shown in Table 2 and were indicated by the shorter 1.90 Å bond length. In brief, the HTAB surfactant molecule arrangements with silica tetrahedra were due to the H-bonds.

https://doi.org/10.1346/CCMN.2018.064109 Published online by Cambridge University Press

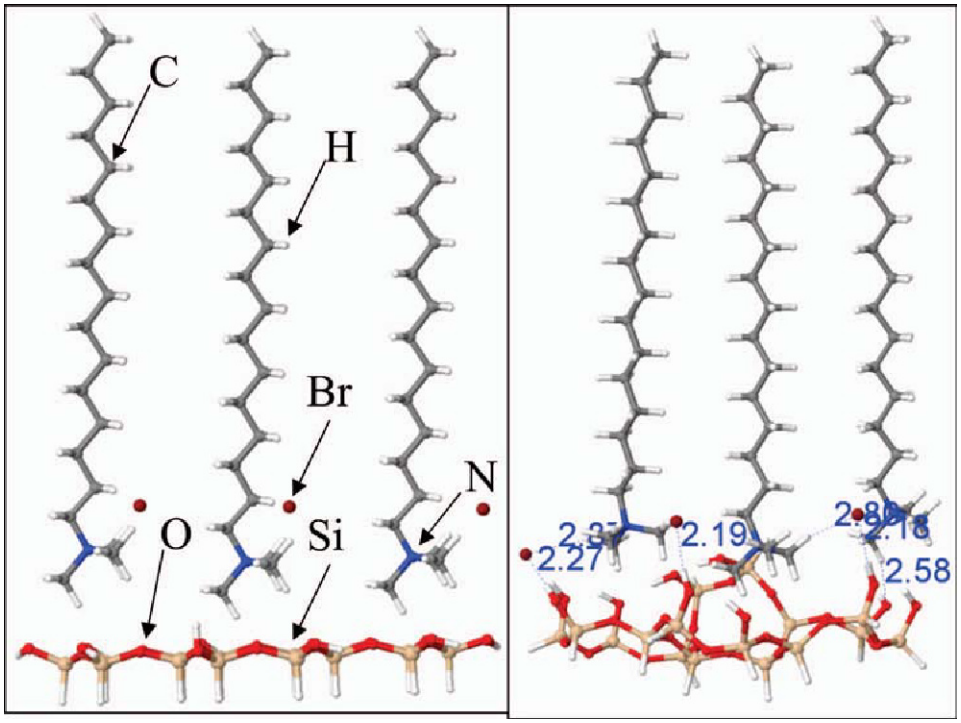

Figure 6. Initial and final states of the neutralized model in an implicit water media. The white (H, white), melon yellow (Si, light gray), red (O, black), gray (C, black), blue (N, black), and baroque red (Br, black) colors represent the elements indicated in parentheses with the grayscale appearance.

The just mentioned model demonstrated that the HTAB surfactant could adsorb to the basal surfaces of sepiolite silica tetrahedra in the presence of Br^- ions.

Table 2. The measured H-bond lengths of defined H-Br and O-H distances for the HTAB/sepiolite model.

— Number of Br^- ions — # of 1st atoms	# of 2nd atoms	Bond lengths for related atoms in Å
H44	Br190	2.22
H46	Br190	2.27
H194	Br190	2.87
O26	H117	2.41
O26	H166	2.99
H168	Br74	2.81
H139	Br74	2.85
H49	Br74	2.19
H195	O10	2.96
O35	H116	2.71
H51	Br164	2.18
H88	Br164	2.80
H259	Br164	2.91
H195	O6	2.58
O52	H208	2.90
O38	H260	2.90
H200	O53	2.58
H91	O40	2.70
H47	O5	1.75
H45	O1	1.88

Thus, a new representative structure was modeled to understand better the behavior of the HTAB surfactant on silica tetrahedra in the absence of Br^- ions. The assumption was that Br^- ions have a free form in an explicit water environment and an initial second model was built accordingly. As shown in Figure 7, the HTA^+ cations were initialized to clarify the effects of the positively charged head group and the hydrophobic interactions of the alkyl chains.

After the vacuum and implicit water media optimizations, one of the HTA^+ molecules was separated from the surface due to the large positive charge (+3) provided by the three HTA^+ in the model. The positive charge resulted in a strong repulsive effect. The positive charge, however, cannot be disengaged completely from the neutral silica surface because of the hydrophobic interactions between aliphatic tails as seen in Figure 7. In addition, three HTAB surfactant tails formed a spiral or helix, which is known as a chain-chain interaction in the experimental literature (Sabah *et al.*, 2002). Not only do the hydrocarbon chains interact, but also the interactions between the HTAB polar head groups and −SiOH can stabilize the model due to the numerous H-bonds. The H-bond distances of between 2.0 and 2.8 Å explain the chain-chain interactions of the HTA^+ surfactant. After the computations, the HTA^+ surfactant molecules tended to form into a bilayer as shown in Figure 7.

https://doi.org/10.1346/CCMN.2018.064109 Published online by Cambridge University Press

Table 3. Calculated binding energies for all models for B97-D/TZVP basis set.

Models	— Vacuum (kJ/mol) —		— *COSMO* (kJ/mol) —	
	B97-D(CP)	B97-D	B97-D(CP)	B97-D
HaZO_SiOSi	−276.79	−298.38	−280.39	−302.41
aZO_SiOSi	−439.00	−471.27	−413.71	−445.09
3HTAB_NaZO	−288.72	−300.63	−304.20	−316.31
3HTAB_SiOSi	−464.56	−485.08	−447.21	−467.16
HTA^+_SiOSi	−350.72	−363.17	−329.48	−341.29
NaZO_2HTAB_SiOSi	−467.01	−482.86	−469.53	−484.59

The model demonstrated that the HTA^+ surfactants could adsorb to the basal surfaces of sepiolite silica tetrahedra with or without Br^- ions. As mentioned in the experimental part of the present study, the HTAB can adsorb to the basal surfaces of sepiolite. After the HTAB organic modification of sepiolite, the number of adsorbed dye molecules increased considerably (Armagan *et al.*, 2003a, 2003b; Ozdemir *et al.*, 2004, 2007). Thus, the model shown in Figure 8 was constructed and computed to explain the interactions between organically modified sepiolite silica tetrahedra with HTAB and acid azo dye 57.

Interactions among sepiolite, HTAB, and acid azo dye 57. The state of the art for theoretical investigations is the interactions between the trimolecular models shown in Figure 8. The main objective here was to demonstrate dye molecule adsorption to the modified sepiolite. Thus, the configuration on the left side of Figure 8 was constructed and was inspired by previous experimental studies (Armagan *et al.*, 2003a; Ozdemir *et al.*, 2004). Ozdemir *et al.* (2014) found that a bilayer structure was formed as dye molecules (acid azo 57) adsorbed to sepiolite or zeolite surfaces. In the present study, the computational calculations were performed using a silanol tetrahedron, two HTAB molecules, and one acid azo dye 57 molecule to produce faster results and use less computer resources.

As shown in Figure 8, three important interactions were observed. First, adsorption of HTAB molecules to

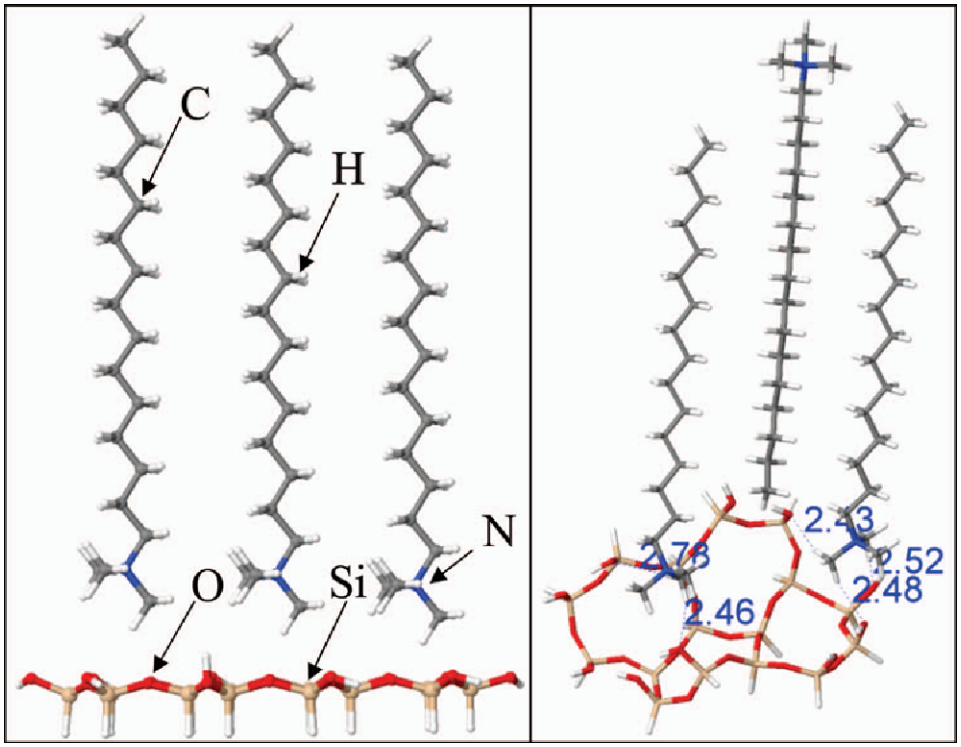

Figure 7. Initial (left) and final (right) states with no ions in an implicit water media. The white (H, white), melon yellow (Si, light gray), red (O, black), gray (C, black), and blue (N, black) colors represent the elements indicated in parentheses with the grayscale appearance.

https://doi.org/10.1346/CCMN.2018.064109 Published online by Cambridge University Press

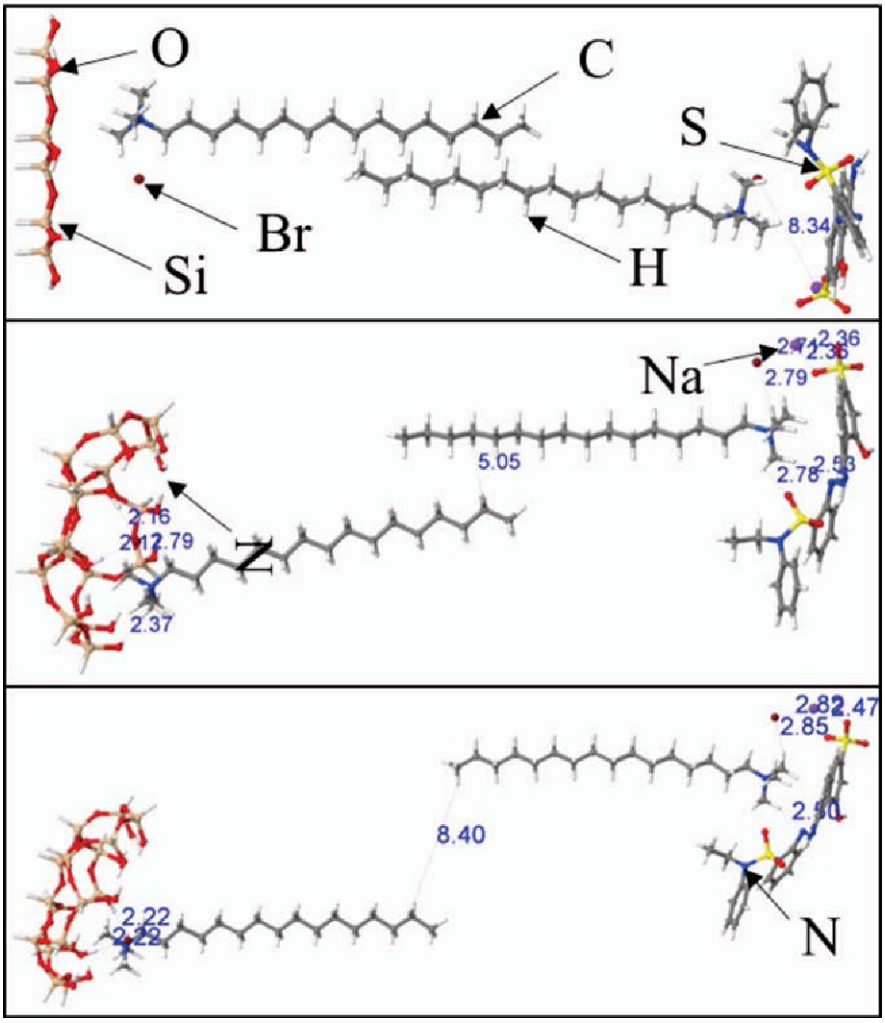

Figure 8. Initial (top) and optimized structures in vacuum (middle) and in an implicit water media (bottom). The white (H, white), red (O, black), blue (N, black), baroque red (Br, black), gray (C, black), yellow (S, gray), and purple (Na, black) colors represent the elements indicated in parentheses with the grayscale appearance.

both sepiolite silanol groups and to acid azo dye 57 was not only due to polar head group effects, but also to hydrophobic interactions between the chains. Second, the interaction between Br^- and Na^+ ions was modeled. The initial distance between the two ions was set to 8.34 Å and was measured to be around 2.7 Å after optimization. The Br^- and Na^+ ions formed a Na^+-Br^- salt complex due to electrostatic interactions in both media. Third, a polar complex between H^+ and Br^- ions formed the acidic H^+-Br^- pair. Fourth, the H-bonds formed between all O and H atoms and were calculated to be <3.0 Å in length as seen in Figure 8. And fifth, the hydrophobic tails, which in the optimization were initially 1.5 Å apart, later moved away from each other to a distance of 8.4 Å. Based on this, the electrostatic interactions were more effective than the hydrophobic interactions. In all of the geometric optimization studies, the modified sepiolite had adsorbed HTAB bilayers and adsorbed acid azo dye 57 molecules.

Interactions between HTAB and acid azo dye 57. The last model was used to examine the interactions between an acid azo dye 57 molecule and three HTAB molecules as shown in Figure 9. A dye molecule and three surfactant molecules were included with the 247 atoms within Na^+ and Br^- ions. All the ions were selected to understand the interactions between Na^+ and Br^- ions, the interactions between HTAB surfactant adsorption and acid azo dye 57, and the interactions among Na^+, Br^-, HTAB, and acid azo dye 57 together as well.

Two important intermolecular interactions were identified. The first interactions were between HTAB surfactant head groups and the H and O atoms of acid azo dye 57. A few H-bonds with bond lengths between

https://doi.org/10.1346/CCMN.2018.064109 Published online by Cambridge University Press

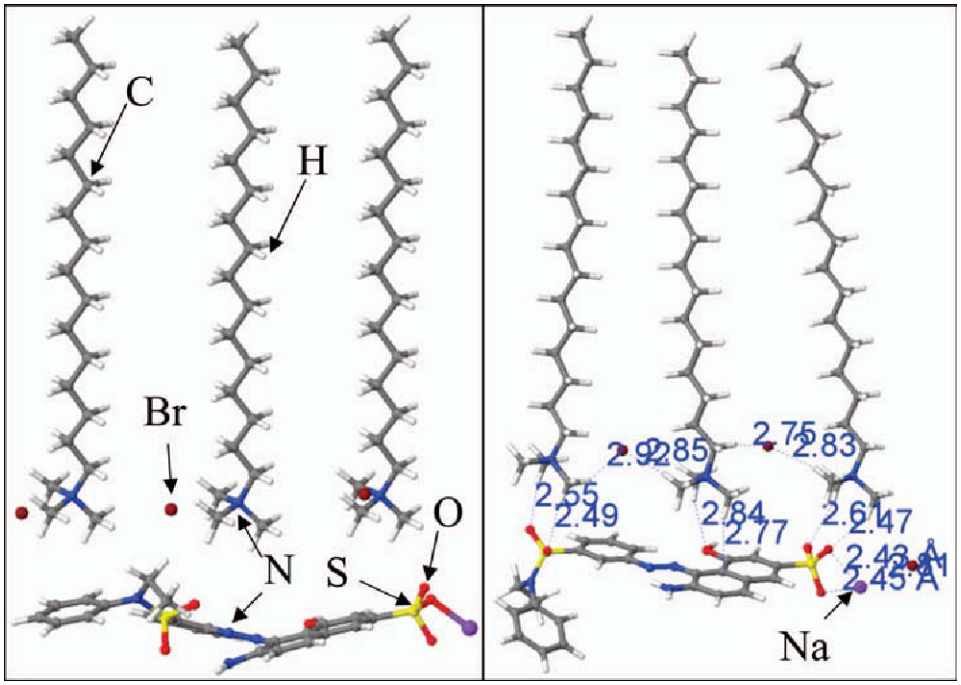

Figure 9. Initial (left) and optimized in vacuum and in implicit water media (right) structures between HTAB and acid azo dye 57. The white (H, white), red (O, black), blue (N, black), baroque red (Br, black), gray (C, black), yellow (S, gray), and purple (Na, black) colors represent the elements indicated in parentheses with the grayscale appearance.

2.35 and 2.84 Å for Br^- ions were measured as shown in Figure 9. Otherwise, the calculated Br-H bond lengths were from 2.75 to 2.89 Å. All distances indicated that the HTAB surfactant molecules within Br^- ions were adsorbed to the surface. Another significant change was the tilt of the ends of the hydrophobic HTAB surfactant tail groups in order to stabilize the structure. The second interaction was the formation of Na^+-Br^- as a salt complex with a Na-Br bond distance of 2.81 Å.

Computed energy results

To understand better the energies after geometric optimization, the adsorption or binding energies of all the mentioned models were calculated using the B97-D/TZVP basis set. After geometric optimization, the binding energies were calculated both in a vacuum and in implicit water media (Table 3). All the negative values indicated that all the models mentioned above could interact with each other. Therefore, not only did HTAB surfactants adsorb to sepiolite and acid azo dye 57 as shown in experimental studies (Armagan *et al.*, 2003a; Ozdemir *et al.*, 2004), but acid azo dye 57 was adsorbed to sepiolite due to the many H-bonds and some electrostatic interactions. Thus, all the models were stabilized in themselves.

As indicated in Table 3, the models with saturated H, Na, and negatively charged acid azo dye 57 were designated HaZO, NaZO, and aZO. The models that had Br atoms, but no ions within the numbered structures were named HTAB and HTA^+. For example, the model designated 3HTAB_NaZO included three HTAB surfactant molecules and had three Br atoms, Na, and an acid azo dye 57 molecule. Likewise, the HTA^+_SiOSi model has a HTAB surfactant molecule and does not contain any ions within the four SiOSi tetrahedra. The last finding is that the strongest interaction in the models was between acid azo dye 57 and the HTAB-modified sepiolite. The CP-corrected interaction energies were computed to be −467.01 and −469.53 kJ/mol in vacuum and in implicit water media, respectively. Likewise, Benkli *et al*. (2005) revealed that after a sufficient number of HTAB molecules were placed on zeolite surfaces to form bilayers, dye molecule uptake increased and the dye bilayer that formed assisted the adsorption of negatively charged dyes to negatively charged zeolite surfaces as indicated in Table 3.

All the interaction energies were negative, all the modeled structures stably interacted with each other, and the models that implicitly contained water were more relaxed and had higher energies as expected. In contrast, the binding energies within the *COSMO* module generally were not larger than that in vacuum media due to the short (~0.2 Å) H-bonds in the media as noted by Karatas *et al*. (2013). For some models, however, the models that implicitly contained water had lower binding energies than the others. For example, the model with the H saturated acid azo dye 57 and aqueous silica tetrahedra, HaZO_SiOSi, had an energy of

https://doi.org/10.1346/CCMN.2018.064109 Published online by Cambridge University Press

4 kJ/mol less than the vacuum phase model in comparison to the models with Br^- ions. Another combination was that between acid azo dye 57 and silica tetrahedra. An H saturated acid azo dye 57 molecule had binding interactions of approximately −300 kJ/mol and −450 kJ/mol for a negatively charged acid azo dye 57 designated aZO_SiOSi (Table 3). The interactions generally increased as the ion number decreased.

CONCLUSIONS

Modification of sepiolite by the HTAB quaternary amine made sepiolite surfaces amenable to the adsorption of dye molecule anionic groups. The results obtained from the present study showed that the HTAB-modified sepiolite had a high dye adsorption capacity. In the theoretical investigations, the following outcomes were determined:

(a) As observed experimentally, the HTAB surfactant in all models could easily adsorb to acid azo dye 57 and silica tetrahedra.

(b) The acid azo dye 57 molecule interacted with silica tetrahedra due to electrostatic interactions.

(c) Hydrophobic interactions between surfactant tails were prominent.

(d) The formation of HTAB bilayers supported acid azo dye 57 molecule adsorption to surfaces due to hydrophobic interactions between HTAB alkyl tails and the H-bonds between H and O atoms.

The experimental studies were in good agreement with the theoretical computations of the DFT studies. A significant increase was calculated for the electrostatic attraction forces between the positive charges of the HTAB molecules and the negative charges of the acid azo 57 dye molecule adsorbed to sepiolite surfaces. All the measured zeta potentials, adsorption experiments, and theoretical computations support this mechanism.

Overall, the theoretical and experimental studies showed that HTAB molecules and acid azo dye 57 molecules could adsorb to sepiolite by physical adsorption. Finally, the present study indicated that sepiolite is indeed a clay mineral with the potential for convenient use in wastewater treatment systems.

ACKNOWLEDGMENTS

This work was supported by Scientific Research Projects Coordination Unit of Istanbul University, Project number 36067. Computing resources used in this work were provided by the National Centre for High Performance Computing of Turkey (UHEM) under grant number 4001782012 and the Informatics Institute of Istanbul Technical University.

REFERENCES

Ahlrichs, R., Bar, M., Haser, M., Horn, H., and Kolmel, C. (1989) Electronic-structure calculations on workstation computers: The program system *Turbomole*. *Chemical Physics Letters*, **162**, 165−169.

Al-Degs, Y., Khraisheh, M.A.M., Allen, S.J., and Ahmad, M.N. (2000) Effect of carbon surface chemistry on the removal of reactive dyes from textile effluent. *Water Research*, **34**, 927−935.

Al-Qodah, Z. (2000) Adsorption of dyes using shale oil ash. *Water Research*, **34**, 4295−4303.

Alvarez, A. (1984) Sepiolite: Properties and uses. Section VI. Industrial uses of sepiolite. Pp. 253−287 in: *Developments in Sedimentology* **37** (A. Singer and E. Galan, editors), Elsevier, New York, doi.org/10.1016/S0070-4571(08)70044-X.

Arbeloa, F.L., Arbeloa, T.L., and Arbeloa, I.L. (1997) Spectroscopy of rhodamine 6G adsorbed on sepiolite aqueous suspensions. *Journal of Colloid Interface Science*, **187**, 105−112.

Armagan, B., Ozdemir, O., Turan, M., and Çelik, M.S. (2003a) Adsorption of negatively charged azo dyes onto surfactant-modified sepiolite. *Journal of Environmental Engineering-Asce*, **129**, 709−715.

Armagan, B., Ozdemir, O., Turan, M., and Çelik, M.S. (2003b) The removal of reactive azo dyes by natural and modified zeolites. *Journal of Chemical Technology & Biotechnology*, **78**, 725−732.

Aznar, A.J., Casal, B., Ruizhitzky, E., Lopezarbeloa, I., Lopezarbeloa, F., Santaren, J., and Alvarez, A. (1992) Adsorption of methylene-blue on sepiolite gels - Spectroscopic and rheological studies. *Clay Minerals*, **27**, 101−108.

Benkli, Y.E., Can, M.F., Turan, M., and Çelik, M.S. (2005) Modification of organo-zeolite surface for the removal of reactive azo dyes in fixed-bed reactors. *Water Research*, **39**, 487−493.

Boys, S.F. and Bernardi, F. (2002) The calculation of small molecular interactions by the differences of separate total energies. Some procedures with reduced errors (Reprinted from Molecular Physics, vol 19, pg 553−566, 1970). *Molecular Physics*, **100**, 65−73.

Brauner, K. and Preisinger, A. (1956) Struktur und entstehung des sepioliths. *Tschermaks mineralogische und petrographische Mitteilungen*, **6**, 120−140.

Can, M.F., Cinar, M., Benli, B., Ozdemir, O., and Çelik, M.S. (2010) Determining the fiber size of nano structured sepiolite using Atomic Force Microscopy (AFM). *Applied Clay Science*, **47**, 217−222.

Chern, J.M. and Huang, S.N. (1998) Study of nonlinear wave propagation theory. 1. Dye adsorption by activated carbon. *Industrial & Engineering Chemistry Research*, **37**, 253−257.

Cinar, M., Ersever, G., Sahbaz, O., and Çelik, M.S. (2011) Sepiolite/calcium interactions in desiccant clay production. *Applied Clay Science*, **53**, 386−394.

Cornejo, J. and Hermosin, M.C. (1988) Evolution of porosity and changes in heat treated lepidocrocite. *Journal of Soil Science*, **39**, 265−274.

Duman, O., Tunc, S., and Polat, T.G. (2015) Adsorptive removal of triarylmethane dye (Basic Red 9) from aqueous solution by sepiolite as effective and low-cost adsorbent. *Microporous and Mesoporous Materials*, **210**, 176−184.

Eichkorn, K., Treutler, O., Öhm, H., Häser, M., and Ahlrichs, R. (1995) Auxiliary basis sets to approximate Coulomb potentials. *Chemical Physics Letters*, **242**, 652−660.

El-Geundi, M. (1991) Homogeneous surface diffusion model of basic dyestuffs onto natural clay in batch adsorbers. *Adsorption Science and Technology*, **8**, 217−225.

Galan, E. (1996) Properties and applications of palygorskite-sepiolite clays. *Clay Minerals*, **31**, 443-453.

Gür, E., Altinisik, A., and Yurdakoc, K. (2017) Preparation and characterization of chitosan/sepiolite bionanocomposites for tetracycline release. *Polymer Composites*, 38, 1810−118.

Hu, Y.Q., Guo, T., Ye, X.S., Li, Q., Guo, M., Liu, H.N., and Wu, Z.J. (2013) Dye adsorption by resins: Effect of ionic strength on hydrophobic and electrostatic interactions. *Chemical Engineering Journal*, **228**, 392–397.

Huang, C.R. and Shu, H.Y. (1995) The reaction-kinetics, decomposition pathways and intermediate formations of phenol in ozonation, UV/O_3 and UV/H_2O_2 processes. *Journal of Hazardous Materials*, **41**, 47–64.

ICI Watercare (1991) Colour in Textile Effluent, Environmental Brief No. 1 in: *Introduction to the Environmental Brief, Colours Textile Dyes Technology Group, ICI*, Manchester, UK.

Juang, R.S., Tseng, R.L., Wu, F.C., and Lee, S.H. (1997) Adsorption behavior of reactive dyes from aqueous solutions on chitosan. *Journal of Chemical Technology and Biotechnology*, **70**, 391–399.

Karatas, D., Tekin, A., and Çelik, M.S. (2013) Adsorption of quaternary amine surfactants and their penetration into the intracrystalline cavities of sepiolite. *New Journal of Chemistry*, **37**, 3936–3948.

Karataş, D., Tekin, A., and Çelik, M.S. (2017) Density functional theory computation of organic compound penetration into sepiolite tunnels. *Clays and Clay Minerals*, **65**, 1–13.

Kasprzhitskii, A., Lazorenko, G., Yavna, V., and Daniel, P. (2016) DFT theoretical and FT-IR spectroscopic investigations of the plasticity of clay minerals dispersions. *Journal of Molecular Structure*, **1109**, 97–105.

Lemic, J., Tomasevic-Canovic, M., Djuricic, M., and Stanic, T. (2005) Surface modification of sepiolite with quaternary amines. *Journal of Colloid Interface Science*, **292**, 11–19.

McKay, G., Blair, H.S., and Gardner, J.R. (1982) Adsorption of dyes on chitin. I. Equilibrium studies. *Journal of Applied Polymer Science*, **27**, 3043–3057.

Meshko, V., Markovska, L., Mincheva, M., and Rodrigues, A.E. (2001) Adsorption of basic dyes on granular acivated carbon and natural zeolite. *Water Research*, **35**, 3357–3366.

Murray, H.H. (1991) Overview – clay mineral applications. *Applied Clay Science*, **5**, 379–395.

Murray, H.H. (2000) Traditional and new applications for kaolin, smectite, and palygorskite: A general overview. *Applied Clay Science*, **17**, 207–221.

Oladipo, A.A., Gazi, M., and Yilmaz, E. (2015) Single and binary adsorption of azo and anthraquinone dyes by chitosan-based hydrogel: Selectivity factor and Box-Behnken process design. *Chemical Engineering Research and Design*, **104**, 264–279.

Ozdemir, O., Armagan, B., Turan, M., and Çelik, M.S. (2004) Comparison of the adsorption characteristics of azo-reactive dyes on mezoporous minerals. *Dyes and Pigments*, **62**, 49–60.

Ozdemir, O., Cinar, M., Sabah, E., Arslan, F., and Çelik, M.S. (2007) Adsorption of anionic surfactants onto sepiolite. *Journal of Hazardous Materials*, **147**, 625–632.

Pelmenschikov, A. and Leszczynski, J. (1999) Adsorption of 1,3,5-trinitrobenzene on the siloxane sites of clay minerals: *Ab Initio* Calculations of molecular models. *The Journal of Physical Chemistry B*, **103**, 6886–6890.

Perdew, J.P., Burke, K., and Ernzerhof, M. (1996) Generalized gradient approximation made simple. *Physical Review Letters*, **77**, 3865–3868.

Post, J.E., Bish, D.L., and Heaney, P.J. (2007) Synchrotron powder X-ray diffraction study of the structure and dehydration behavior of sepiolite. *American Mineralogist*, **92**, 91–97.

Rearick, W.A., Farias, L.T., and Goettsch, H.B.G. (1997) Water and salt reuse in the dyehouse. *Textile Chemist and Colorist*, **29**, 10–19.

Ruiz-Hitzky, E. (2001) Molecular access to intracrystalline tunnels of sepiolite. *Journal of Materials Chemistry*, **11**, 86–91.

Rytwo, G., Nir, S., Crespin, M., and Margulies, L. (2000) Adsorption and interactions of methyl green with montmorillonite and sepiolite. *Journal of Colloid Interface Science*, **222**, 12–19.

Sabah, E. and Çelik, M.S. (2002) Adsorption mechanism of quaternary amines by sepiolite. *Separation Science and Technology*, **37**, 3081–3097.

Sabah, E., Kara, M., Hançer, M., and Çelik, M.S., (1998) Adsorption mechanism of organic and inorganic ions by clay absorbent: Sepiolite. Presented at the *Society for Mining, Metallurgy, and Exploration, Inc. Annual Meeting in Orlando, Florida-USA, March 9-11, 1998*.

Sabah, E., Turan, M., and Çelik, M.S. (2002) Adsorption mechanism of cationic surfactants onto acid- and heat-activated sepiolites. *Water Research*, **36**, 3957–3964.

Santaren, J. (1993) European market developments for absorbent clays. *Industrial Minerals*, **304**, 35–47.

Santaren, J., Sanz, J., and Ruiz-Hitzky, E. (1990) Structural fluorine in sepiolite. *Clays and Clay Minerals*, **38**, 63–68.

Shuali, U., Bram, L., Steinberg, M., and Yariv, S. (1989) Infrared study of the thermal treatment of sepiolite and palygorskite saturated with organic amines. *Thermochimica Acta*, **148**, 445–456.

Stefan, G. (2006) Semiempirical GGA-type density functional constructed with a long-range dispersion correction. *Journal of Computational Chemistry*, **27**, 1787–1799.

Suarez, M. and Garcia-Romero, E. (2012) Variability of the surface properties of sepiolite. *Applied Clay Science*, **67–68**, 72–82.

Sun, G. and Xu, X. (1997) Sunflower stalks as adsorbents for color removal from textile wastewater. *Industrial & Engineering Chemistry Research*, **36**, 808–812.

Wu, J., Eiteman, M.A., and Law, S.E. (1998) Evaluation of membrane filtration and ozonation processes for treatment of reactive-dye wastewater. *Journal of Environmental Engineering-Asce*, **124**, 272–277.

Yoo, E.S., Libra, J., and Adrian, L. (2001) Mechanism of decolorization of azo dyes in anaerobic mixed culture. *Journal of Environmental Engineering*, **127**, 844–849.

(*Received 13 June 2017; revised 21 July 2018; Ms. 1184; AE: A.G. Kalinichev*)